Eur. Phys. J. C (2019) 79:522
https://doi.org/10.1140/epjc/s10052-019-7033-8

THE EUROPEAN PHYSICAL JOURNAL C

Regular Article - Theoretical Physics

Predictive scotogenic model with flavor dependent symmetry

Zhi-Long Han[1,a], **Weijian Wang**[2,b]

[1] School of Physics and Technology, University of Jinan, Jinan 250022, Shandong, China
[2] Department of Physics, North China Electric Power University, Baoding 071003, China

Received: 28 March 2019 / Accepted: 8 June 2019 / Published online: 18 June 2019

Abstract In this paper, we propose a viable approach to realise two texture-zeros in the scotogenic model with flavor dependent $U(1)_{B-2L_\alpha-L_\beta}$ gauge symmetry. These models are extended by two right-handed singlets N_{Ri} and two inert scalar doublets η_i, which are odd under the dark Z_2 symmetry. Among all the six constructed textures, texture A_1 and A_2 are the only two allowed by current experimental limits. Then choosing texture A_1 derived from $U(1)_{B-2L_e-L_\tau}$, we perform a detail analysis on the corresponding phenomenology such as predictions of neutrino mixing parameters, lepton flavor violation, dark matter and collider signatures. One distinct nature of such model is that the structure of Yukawa coupling $\bar{L}\tilde{\eta}N_R$ is fixed by neutrino oscillation data, and can be further tested by measuring the branching ratios of charged scalars $\eta^{\pm}_{1,2}$.

1 Introduction

It is well known that the standard model (SM) needs extensions to accommodate two missing spices: the tiny but nozero neutrino masses and the cosmological dark matter (DM) candidates. One way of incorporating above two issues in a unified framework is the scotogenic model [1–3], where neutrinos are radiatively generated and the DM field serves as intermediate messengers propagating inside the loop diagram. With all new particles around TeV scale, the scotogenic model leads to testable phenomenologies [4–31]. Therefore, viable models are extensively studies in recent years [32].

On the other hand, the understanding of the leptonic flavor structure is still one of the major open questions in particle physics. The consensus is that the leptonic mass texture is tightly restricted under the present experimental data. An attractive approach is to consider two texture-zeros in neutrino mass matrix (M_ν) so that the number of parameters in the Lagrangian is reduced [33]. The phenomenological analysis of two texture-zeros models have been studied in Refs. [34,35]. Among fifteen logically patterns, seven of them are compatible to the low-energy experimental data.

On the theoretical side, the simplest way of realizing texture-zeros is to impose the discrete Z_N flavor symmetry [36]. However, it might be more appealing to adopt gauge symmetries instead of discrete ones, because the latter may be treated as the residual of $U(1)$ gauge symmetry. It is noted that one can not set any restriction on lepton mass matrix by means of fields with flavor universal charges. Thus the flavor dependent $U(1)$ gauge symmetry is the reasonable choice. Along this thought of idea, specific models are considered in the context of seesaw mechanisms. In Ref. [37], the two texture-zeros are realized based on the anomaly-free $U(1)_X$ gauge symmetry with $X \equiv B - \sum x_\alpha L_\alpha (\alpha = e, \mu, \tau)$ being the linear combination of baryon number B and the lepton numbers L_α per family. In Ref. [38], more solutions are found in the type-I and/or III seesaw framework.

It is then natural to ask, if predictive texture-zeros in M_ν can be realized in the scotogenic scenario and several attempts have been made in this direction. For example, one texture-zero is recently considered in Ref. [39]. Texture B_1-B_4 have been discussed in a model-independent way in Ref. [40]. Texture C is obtained by introducing $U(1)_{L_\mu-L_\tau}$ gauge symmetry [41–44]. Texture B_2 is realised with $U(1)_{L_e+L_\mu-L_\tau}$ gauge symmetry in Ref. [45]. If the quark flavor is also flavor dependent, e.g., $U(1)_{xB_3-xL_e-L_\mu+L_\tau}$, then one can further interpret the R_K anomaly with texture A_1 [46]. Other viable two texture-zeros are systematically realised in Ref. [47] by considering the $U(1)_{B-2L_\alpha-L_\beta}$ gauge symmetry with three right-handed singlets. In this paper, we provide another viable approach. Under the same flavor dependent $U(1)_{B-2L_\alpha-L_\beta}$ gauge symmetry, we introduce only two right-handed singlets but two inert scalars, leading to different texture-zeros compared with Ref. [47]. In aspect of predicted phenomenology, the texture B_1 con-

[a] e-mail: sps_hanzl@ujn.edu.cn
[b] e-mail: wjnwang96@aliyun.com

sidered in Ref. [47] is marginally allowed by current Planck result for $\sum m_i < 0.12$ eV [48], we thus consider texture A_1 with latest neutrino oscillation data [49] as the benchmark model. In this case, the gauge symmetry is $U(1)_{B-2L_e-L_\tau}$ in our approach.

The rest of this paper is organised as follows. Start with classic scotogenic model in Sect. 2, we first discuss the realization of texture-zeros in scotogenic model with $U(1)_{B-2L_\alpha-L_\beta}$ gauge symmetry in a general approach. Then the texture A_1 derived from $U(1)_{B-2L_e-L_\tau}$ is explained in detail. The corresponding phenomenological predictions, such as neutrino mixing parameters, lepton flavor violation rate, dark matter and highlights of collider signatures are presented in Sect. 3. Finally, conclusions are summarised in Sect. 4.

2 The model setup

2.1 Classic scotogenic model

In the classic scotogenic model proposed by Ma [1], three right-handed fermion singlets $N_{Ri}(i = 1 \sim 3)$ and an inert scalar doublet field $\eta = (\eta^+, \eta^0)$ are added to the SM. In addition, a discrete Z_2 symmetry is imposed for the new fields in order to forbid the tree-level neutrino Yukawa interaction and stabilize the DM candidate. The relevant interactions for neutrino masses generation are given by

$$\mathcal{L} \supset h_{\alpha i}\overline{L}_\alpha\tilde{\eta}N_{Ri} + \frac{1}{2}M_N\overline{N}^c_R N_R + \frac{1}{2}\lambda(\Phi^\dagger\eta)^2 + \text{h.c.}. \tag{1}$$

The mass matrix M_N can be diagonalized by an unitary matrix V satisfying

$$V^T M_N V = \hat{M}_N \equiv \text{diag}(M_{N1}, M_{N2}, M_{N3}). \tag{2}$$

Due to the Z_2 symmetry, the neutrino masses are generated at one-loop level, as show in left pattern of Fig. 1. The neutrino mass matrix can be computed exactly, i.e.

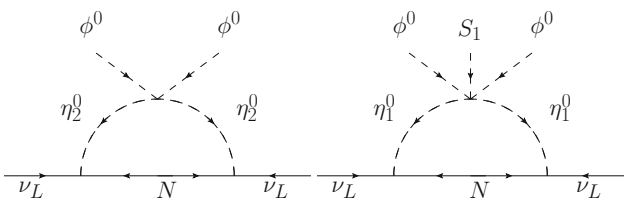

Fig. 1 Radiative neutrino mass at one-loop. Left pattern is for classic scotogenic model, while right pattern is the additional contribution in our models

$$(M_\nu)_{\alpha\beta} = \frac{1}{32\pi^2}\sum_k h_{\alpha i}V_{ik}h_{\beta j}V_{jk}M_{Nk} \times\left[\frac{m_R^2}{m_R^2-M_{Nk}^2}\log\left(\frac{m_R^2}{M_{Nk}^2}\right) - \frac{m_I^2}{m_I^2-M_{Nk}^2}\log\left(\frac{m_I^2}{M_{Nk}^2}\right)\right] \tag{3}$$

where m_R and m_I are the masses of $\sqrt{2}\Re\eta^0$ and $\sqrt{2}\Im\eta^0$. If we assume $m_0^2 \equiv (m_R^2 + m_I^2)/2 \gg M_{Nk}^2$, M_ν are then given by

$$\begin{aligned}(M_\nu)_{\alpha\beta} &\simeq -\frac{1}{32\pi^2}\frac{\lambda v^2}{m_0^2}\sum_k h_{\alpha i}V_{ik}h_{\beta j}V_{jk}M_{Nk} \\ &= -\frac{1}{32\pi^2}\frac{\lambda v^2}{m_0^2}(hM_N h^T)_{\alpha\beta}\end{aligned} \tag{4}$$

The neutrino mass matrix M_ν is diagonalized as

$$U_{\text{PMNS}}^T M_\nu U_{\text{PMNS}} = \hat{m}_\nu \equiv \text{diag}(m_1, m_2, m_3), \tag{5}$$

where U_{PMNS} is the neutrino mixing matrix denoted as

$$U_{\text{PMNS}} = \begin{pmatrix} c_{12}c_{13} & s_{12}c_{13} & s_{13} \\ -c_{12}s_{23}s_{13} - s_{12}c_{23}e^{-i\delta} & -s_{12}s_{23}s_{13} + c_{12}c_{23}e^{-i\delta} & s_{23}c_{13} \\ -c_{12}c_{23}s_{13} + s_{12}s_{23}e^{-i\delta} & -s_{12}c_{23}s_{13} - c_{12}s_{23}e^{-i\delta} & c_{23}c_{13} \end{pmatrix} \times \text{diag}(e^{i\rho}, e^{i\sigma}, 1) \tag{6}$$

Here, we define $c_{ij} = \cos\theta_{ij}$ and $s_{ij} = \sin\theta_{ij}$ $(ij = 12, 23, 13)$ for short, δ is the Dirac phase and ρ, σ are the two Majorana phases as in Ref. [34].

2.2 Two texture-zeros in scotogenic model

In this section, we demonstrate a class of scotogenic models with $G_{SM} \times U(1)_{B-2L_\alpha-L_\beta} \times Z_2$ gauge symmetry where two texture-zero structures in M_ν are successfully realized. The particle content and corresponding charge assignments are listed in Table 1. In the fermion sector, we introduce two right-handed $SU(2)_L$ singlets N_{R1} and N_{R2} and assume they carry the same no-zero $B - 2L_\alpha - L_\beta$ charges as two of SM leptons respectively. Noticeably, if one further introduce one additional N_{R3} with zero $B - 2L_\alpha - L_\beta$ charge, the approach considered in Ref. [47] are then reproduced. In terms of gauged $U(1)_{B-2L_\alpha-L_\beta}$ symmetry, the anomaly free conditions should be considered first and we find all anomalies are zero because

$$\begin{aligned}&[SU(3)_c]^2U(1)_X : 3\times\frac{1}{2}\left(\frac{2}{3}-\frac{1}{3}-\frac{1}{3}\right) = 0 \\ &U(1)_Y[U(1)_X]^2 : 3\left[6\left(\frac{1}{6}\right)-3\left(\frac{2}{3}\right)-3\left(\frac{1}{3}\right)\right]\left(\frac{1}{3}\right)^2 \\ &\quad+\left[2\left(-\frac{1}{2}\right)-(-1)\right]\left[(-1)^2+(-2)^2\right] = 0 \\ &[SU(2)_L]^2U(1)_X : \frac{1}{2}\left[3\times 3\left(\frac{1}{3}\right)+(-1)+(-2)\right] = 0\end{aligned}$$

Table 1 Particle content and corresponding charge assignments

Group	Lepton fields								Scalar fields				
	L_α	$\ell_{\alpha R}$	L_β	$\ell_{\beta R}$	L_γ	$\ell_{\gamma R}$	N_{R1}	N_{R2}	Φ	η_1	η_2	S_1	S_2
$SU(2)_L$	2	1	2	1	2	1	0	0	2	2	2	1	1
$U(1)_Y$	$-\frac{1}{2}$	-1	$-\frac{1}{2}$	-1	$-\frac{1}{2}$	-1	1	1	$\frac{1}{2}$	$\frac{1}{2}$	$\frac{1}{2}$	0	0
Z_2	$+$	$+$	$+$	$+$	$+$	$+$	$-$	$-$	$+$	$-$	$-$	$+$	$+$
$U(1)_{B-2L_\alpha-L_\beta}$	-2	-2	-1	-1	0	0	-1	-2	0	-1	0	2	3

$$
\begin{aligned}
&[U(1)_Y]^2U(1)_X : 3\left[6\left(\frac{1}{6}\right)^2 - 3\left(\frac{2}{3}\right)^2 - 3\left(\frac{1}{3}\right)^2\right]\left(\frac{1}{3}\right)\\
&\quad + \left[2\left(-\frac{1}{2}\right)^2 - (-1)^2\right](-1-2) = 0\\
&U(1)_X^3 : 2(-1)^3 - 2(-1)^3 + 2(-2)^3 - 2(-2)^3 = 0\\
&[\text{Gravity}]^2U(1)_X : 2(-1) - 2(-1) + 2(-2) - 2(-2) = 0
\end{aligned}
\tag{7}
$$

Let us now discuss the scotogenic realizations of two texture-zeros in M_ν. With two N_R components, h and M_N are 3×2 and 2×2 matrices respectively. From Eq. (4), it is clear that the texture-zeros of M_ν can be attributed to the texture-zeros in h and M_N matrices. In the original scotogenic model with an inert scalar doublet η and two N_R fields, the charge assignments for $U(1)_{B-2L_\alpha-L_\beta}$ gauge symmetry give rise to only two Yukawa terms for $h_{\alpha i}\overline{L}_\alpha\tilde{\eta}N_{Ri}(\alpha = e,\mu,\tau, i = 1,2)$. In this case, at least two texture-zeros are placed in the same line of h matrix, being therefore excluded experimentally. In order to accommodate the realistic neutrino mixing data, the scotogenic model are extended where, in scalar sector, two inert doublet η_1 and η_2 are introduced (see Table 1). In addition, two scalar singlet S_1 and S_2 are added so that $U(1)_{B-2L_\alpha-L_\beta}$ symmetry is spontaneously breaking after $S_{1,2}$ get the vacuum expectation value (VEV) $\langle S_{1,2}\rangle = v_{1,2}/\sqrt{2}$. Note that N_{Ri} and η_i are odd under the discrete Z_2 symmetry. Since we have two inert scalars, the relevant scalar interactions for the loop-induced neutrino masses is given by

$$
\mathcal{L}_S \supset \frac{\lambda}{\Lambda}(\Phi^\dagger\eta_1)^2S_1 + \lambda'(\Phi^\dagger\eta_2)^2 + \left(\lambda_1(\eta_2^\dagger\eta_1)S_1^*S_2 + \text{h.c.}\right), \tag{8}
$$

where Λ is a new high energy scale and the first term is a dimension-five operator guaranteed by the accidental $U(1)_{B-2L_\alpha-L_\beta}$ symmetry. One can achieve the effective operator by simply adding a new scalar singlet $\rho \sim (1,0,1,-)$ so that in scalar sector $\mathcal{L}_S \supset \mu(\Phi^\dagger\eta_1)\rho^\dagger + \mu'\rho^2S_1$ is allowed. Then the effective interaction $\lambda(\Phi^\dagger\eta_1)^2S_1/\Lambda$ is obtained by integrate the ρ field out of $\mathcal{L}_S$ sector. In the following analysis, we adopt the expression of effective operator in Eq. (8) and do not consider its specific realization in detail. After $S_{1,2}$ develop VEVs, the λ_1-term will induce mixing between η_1 and η_2. In following studies, we set $\lambda_1 = 0$, thus no mixing between η_1 and η_2 for simplicity.

The neutrinos acquire their tiny masses radiatively though the one-loop diagrams depicted in Fig. 1. As a case study, we consider the $U(1)_{B-2L_e-L_\tau}$ gauge symmetry, under which the flavor dependent Yukawa interactions are given by

$$
\begin{aligned}
-\mathcal{L}_Y = {}& h_{\mu1}\bar{L}_\mu\tilde{\eta}_1N_{R1} + h_{\tau2}\bar{L}_\tau\tilde{\eta}_1N_{R2}\\
&+ f_{\tau1}\bar{L}_\tau\tilde{\eta}_2N_{R1} + f_{e2}\bar{L}_e\tilde{\eta}_2N_{R2}\\
&+ y_{11}\overline{N_{R1}^c}N_{R1}S_1 + y_{12}(\overline{N_{R1}^c}N_{R2}\\
&+ \overline{N_{R2}^c}N_{R1})S_2 + \text{h.c.}.
\end{aligned}
\tag{9}
$$

From the charge assignment, the texture of above Yukawa couplings are

$$
h = \begin{pmatrix} 0 & 0\\ h_{\mu1} & 0\\ 0 & h_{\tau2}\end{pmatrix},\quad f = \begin{pmatrix} 0 & f_{e2}\\ 0 & 0\\ f_{\tau1} & 0\end{pmatrix},\quad y = \begin{pmatrix} y_{11} & y_{12}\\ y_{12} & 0\end{pmatrix}. \tag{10}
$$

Therefore, the neutrino mass matrix is formulated by two different contribution coming from η_1 and η_2, namely,

$$
(M_\nu) \propto hM_Nh^T + fM_Nf^T, \tag{11}
$$

with further assumption $\Lambda = \langle S_1\rangle$ and $\lambda/m_{\eta_1}^2 = \lambda'/m_{\eta_2}^2$. Provided all the element in M_N to be equal, then from the texture structure in Eq. (10) and using Eq. (11) we have the M_ν as

$$
M_\nu \propto \begin{pmatrix} 0 & 0 & f_{e2}f_{\tau1}\\ 0 & h_{\mu1}^2 & h_{\mu1}h_{\tau2}\\ f_{e2}f_{\tau1} & h_{\mu1}h_{\tau2} & f_{\tau1}^2\end{pmatrix}, \tag{12}
$$

which is texture A_1 allowed by experimental data [34,35]. Other possible realizations of two-zero textures with $U(1)_{B-2L_\alpha-L_\beta}$ can then be easily obtained in a similar approach. In Table 2, we summarize all the six textures realised by $U(1)_{B-2L_\alpha-L_\beta}$ in our approach. According to Ref. [35], texture A_1 and A_2 predict $\sum m_i \sim 0.07$ eV, hence they are allowed by Planck limit $\sum m_i < 0.12$ eV [48]. Texture B_3 and B_4 predict $\sum m_i \gtrsim 0.15$ eV, thus they are marginally allowed if certain mechanism is introduced to modify cosmology data. Texture D_1 and D_2 are

Table 2 Two texture-zeros and corresponding $U(1)_{B-2L_\alpha-L_\beta}$ symmetry. Here, $\times$ denotes a nonzero matrix element

Texture of M_ν	Group	Texture of M_ν	Group	Status
$A_1: \begin{pmatrix} 0 & 0 & \times \\ 0 & \times & \times \\ \times & \times & \times \end{pmatrix}$	$U(1)_{B-2L_e-L_\tau}$	$A_2: \begin{pmatrix} 0 & \times & 0 \\ \times & \times & \times \\ 0 & \times & \times \end{pmatrix}$	$U(1)_{B-2L_e-L_\mu}$	Allowed
$B_3: \begin{pmatrix} \times & 0 & \times \\ 0 & 0 & \times \\ \times & \times & \times \end{pmatrix}$	$U(1)_{B-2L_\mu-L_\tau}$	$B_4: \begin{pmatrix} \times & \times & 0 \\ \times & \times & \times \\ 0 & \times & 0 \end{pmatrix}$	$U(1)_{B-2L_\tau-L_\mu}$	Marginally allowed
$D_1: \begin{pmatrix} \times & \times & \times \\ \times & 0 & 0 \\ \times & 0 & \times \end{pmatrix}$	$U(1)_{B-2L_\mu-L_e}$	$D_2: \begin{pmatrix} \times & \times & \times \\ \times & \times & 0 \\ \times & 0 & 0 \end{pmatrix}$	$U(1)_{B-2L_\tau-L_e}$	Excluded

Table 3 Same as 2, but for one texture-zero

Texture of M_ν	Group	Texture of M_ν	Group	Status texture of M_ν	Group
$\begin{pmatrix} 0 & \times & \times \\ \times & \times & \times \\ \times & \times & \times \end{pmatrix}$	$U(1)_{B-2L_e-L_{\mu,\tau}}$	$\begin{pmatrix} \times & \times & \times \\ \times & 0 & \times \\ \times & \times & \times \end{pmatrix}$	$U(1)_{B-2L_\mu-L_{e,\tau}}$	$\begin{pmatrix} \times & \times & \times \\ \times & \times & \times \\ \times & \times & 0 \end{pmatrix}$	$U(1)_{B-2L_\tau-L_{e,\mu}}$

already excluded by neutrino oscillation data. The following phenomenological predictions are based on texture A_1 with $U(1)_{B-2L_e-L_\tau}$.

Note if $\lambda_1 \neq 0$, hence mixing between η_1 and η_2 exists, then new contributions as $hM_N f^T + fM_N h^T$ to neutrino masses are possible. In this way, the resulting neutrino mass matrix will only have one texture-zero [50], thus less constrained and less predictive than the two texture-zero. The obtained one texture-zeros are presented in Table 3, which are all allowed by neutrino oscillation data [50]. Since two different gauge symmetry lead to same one texture-zero, it is then not possible to distinguish them only by precise neutrino oscillation measurements.

In the mass eigenstate of heavy Majorana fermion N_i, the corresponding Yukawa couplings with leptons are easily obtained by

$$h' = hV = \begin{pmatrix} 0 & 0 \\ h_{\mu 1}V_{11} & h_{\mu 1}V_{12} \\ h_{\tau 2}V_{21} & h_{\tau 2}V_{22} \end{pmatrix},$$
$$f' = fV = \begin{pmatrix} f_{e2}V_{21} & f_{e2}V_{22} \\ 0 & 0 \\ f_{\tau 1}V_{11} & f_{\tau 1}V_{12} \end{pmatrix}. \quad (13)$$

For the Z_2-even scalars, the CP-even scalars in weak-basis $(\sqrt{2}\Re\Phi^0, \sqrt{2}\Re S_1, \sqrt{2}\Re S_2)$ mix into mass-basis (h, H_1, H_2) with mass spectrum $M_h \sim M_{H_1} < M_{H_2}$. Without loss of generality, we further assume the mixing angle between (h, H_1) to be α and vanishing mixing angles between H_2 and h/H_1 for simplicity. Mass of H_2 is fixed to be $m_{H_2} = 10$ TeV. The would-be Goldstone boson Φ^+, $\sqrt{2}\Im\Phi^0$, $\sqrt{2}\Im S_2$ are absorbed by gauge boson W^+, Z, Z' respectively, leaving $\sqrt{2}\Im S_1$ a pseudo-Goldstone, e.g., Majoron J. This Majoron can be assigned to the spontaneous breaking of the global $U(1)_L$ lepton number symmetry, under which $L, \ell, N_R \sim 1, S_{1,2} \sim -2$. All the renormalizable interactions preserve this global symmetry, but the effective interaction $\lambda(\Phi^\dagger\eta_1)^2 S_1/\Lambda$ clearly breaks this $U(1)_L$ symmetry. This term will induce an effective mass term for the Majoron at one loop level, with $m_J \sim \lambda v^2/(4\pi\Lambda)$. Typically, for $\Lambda \sim 10$ TeV and $\lambda \sim 10^{-10}$ to acquire correct neutrino masses [51], we have $m_J \sim 10^{-2}$ eV. Due to the charge assignment, the Majoron here does not mix with SM Goldstone bosons, thus it is a pure singlet under SM gauge group. From Eq. (9), we know that this Majoron only directly couples to the inert N_R, and the Yukawa coupling $\bar{L}\tilde{\eta}N_R$ could mediate Majoron coupling to leptons at one loop level. For 10^{-2} eV scale Majoron J, it can only decay into light neutrinos. Since texture of M_ν in Eq. (4) is derived by $m_0^2 \gg M_{Nk}^2$, only fermion DM is allowed in this paper.

3 Phenomenology

3.1 Neutrino mixing

As shown in the previous section, the flavor dependent $U(1)_{B-2L_e-L_\tau}$ symmetry leads to texture A_1 [34,35]. Since $(M_\nu)_{ee} = 0$, the predicted effective Majorana neutrino mass $\langle m\rangle_{ee}$ is exactly zero for the neutrinoless double-beta decay. Therefore, only normal hierarchy is allowed in this model [52,53]. Following the procedure in Ref. [34], we now update the predictions of neutrino oscillation data with latest global analysis results [49].

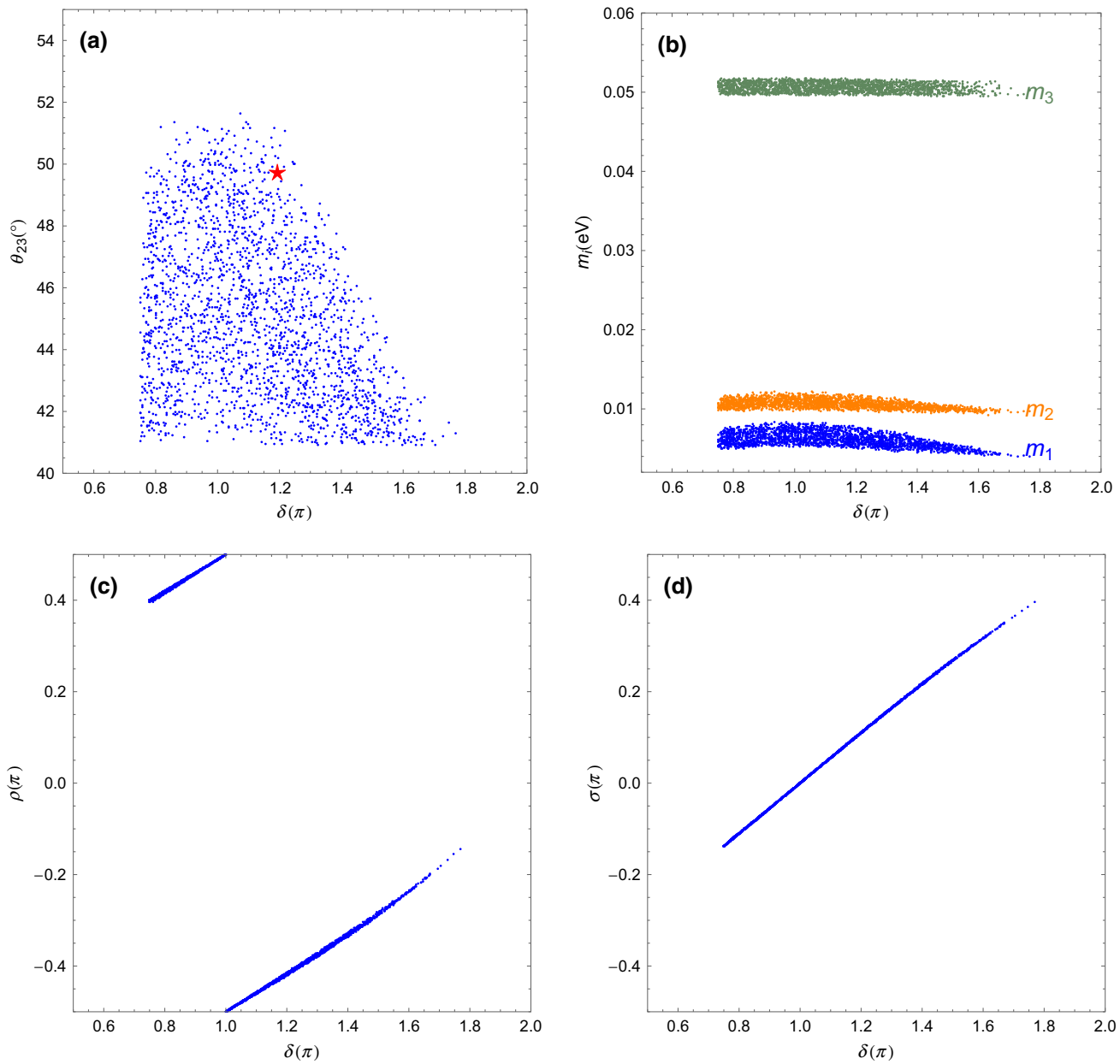

Fig. 2 Allowed samples of A_1 texture with neutrino oscillation data varied in 3σ range of Ref. [49]. In pattern **a**, the red star ★ stands for the best fit point from global analysis

In Fig. 2, we show the scanning results of texture A_1. It is worth to note that the best fit value of neutrino oscillation parameters by global analysis [49] is only marginally consistent with predictions of texture A_1, which is clearly seen in Fig. 2a. From Fig. 2b, we obtain that $m_1 \sim 0.007$ eV, $m_2 \sim 0.01$ eV, and $m_3 \approx \sqrt{\Delta m^2} \sim 0.05$ eV. The resulting sum of neutrino mass is then $\sum m_i \sim 0.07$ eV, thus it satisfies the bound from cosmology, i.e., $\sum m_i < 0.12$ eV [48,54]. The Dirac phase should fall in the range $\delta \in [0.75\pi, 1.77\pi]$, meanwhile Fig. 2c, d indicate that $\rho \approx \frac{\delta}{2}$ and $\sigma \approx \frac{\delta}{2} - \frac{\pi}{2}$.

Instead of the marginally best fit neutrino oscillation parameters, we take $\delta = \pi$ and $\theta_{23} = 46^\circ$ with other oscillation parameters being the best fit value in Ref. [49] as the benchmark point for illustration, which leads to the following neutrino mass structure

$$M_\nu = \begin{pmatrix} 0 & 0 & 0.0110 \\ 0 & 0.0293 & 0.0219 \\ 0.0110 & 0.0219 & 0.0256 \end{pmatrix} \text{ eV} \tag{14}$$

By comparing the analytic M_ν in Eq. (12) and the numerical M_ν in Eq. (14), one can easily reproduce the observed neutrino oscillation data by requiring

$$\frac{h_{\tau 2}}{h_{\mu 1}} : \frac{f_{\tau 1}}{h_{\mu 1}} : \frac{f_{e2}}{h_{\mu 1}} = \frac{(M_\nu)_{\mu\tau}}{(M_\nu)_{\mu\mu}} : \sqrt{\frac{(M_\nu)_{\tau\tau}}{(M_\nu)_{\mu\mu}}} : \frac{(M_\nu)_{e\tau}}{\sqrt{(M_\nu)_{\mu\mu}(M_\nu)_{\tau\tau}}} \simeq 0.745 : 0.933 : 0.401. \quad (15)$$

Hence, we can take $h_{\mu 1}$ as free parameters and determine the other three Yukawa coupling by using above ratios. The overall neutrino mass scale is then determined by $\lambda v^2 M_N h_{\mu 1}^2/(32\pi^2 m_0^2) \approx 0.0293$ eV.

3.2 Lepton flavor violation

The new Yukawa interactions of the form $\bar{L}\tilde{\eta} N_R$ will contribute to lepton flavor violation (LFV) processes [55,56]. In this work, we take the radiative decay $\ell_i \to \ell_j \gamma$ for illustration. Generally, the Yukawa couplings are tightly constrained by LFV. With flavor dependent $U(1)_{B-2L_e-L_\tau}$ symmetry and vanishing mixing angle θ, it is clear from Eq. (9) that $\eta_1^\pm(\eta_2^\pm)$ will only induce $\tau \to \mu\gamma(\tau \to e\gamma)$ at one-loop level. It is worth to note that the most stringent $\mu \to e\gamma$ decay is missing at one-loop level. Hence, if the ongoing experiments observe $\tau \to \mu(e)\gamma$ but no $\mu \to e\gamma$, this model will be favored. The corresponding branching ratios are calculated as

$$\begin{aligned}
&\mathrm{BR}(\tau \to \mu\gamma) \\
&= \frac{3\alpha}{64\pi G_F^2} \left| \sum_{i=1}^{2} \frac{(h_{\mu 1} V_{1i})(h_{\tau 2} V_{2i})^*}{M_{\eta_1}^2} F\left(\frac{M_{Ni}^2}{M_{\eta_1}^2}\right) \right|^2 \mathrm{BR}(\tau \to \mu \nu_\tau \bar{\nu}_\mu), \\
&\mathrm{BR}(\tau \to e\gamma) \\
&= \frac{3\alpha}{64\pi G_F^2} \left| \sum_{i=1}^{2} \frac{(f_{e2} V_{2i})(f_{\tau 1} V_{1i})^*}{M_{\eta_2}^2} F\left(\frac{M_{Ni}^2}{M_{\eta_2}^2}\right) \right|^2 \mathrm{BR}(\tau \to e \nu_\tau \bar{\nu}_e),
\end{aligned} \quad (16)$$

where the loop function $F(x)$ is

$$F(x) = \frac{1 - 6x + 3x^2 + 2x^3 - 6x^2 \ln x}{6(1-x)^4}. \quad (17)$$

In the limit of degenerate M_N, we have

$$\mathrm{BR}(\tau \to \ell\gamma) \propto \left| \sum_{i=1}^{2} V_{1i} V_{2i}^* \right|^2 = |(V V^\dagger)_{12}|^2 = 0, \quad (18)$$

where in the last step, we have considered the fact that V is an unitary matrix. Therefore, cancellations between the contributions of two N_i are also expected even in the case of nearly degenerate M_N. In Fig. 3, we show the predictions for $\tau \to \mu\gamma$ and $\tau \to e\gamma$. Although constraint on $\mathrm{BR}(\tau \to e\gamma)$ is slightly more stringent than $\mathrm{BR}(\tau \to \mu\gamma)$, the predicted $\mathrm{BR}(\tau \to e\gamma)$ is much smaller than $\mathrm{BR}(\tau \to \mu\gamma)$. It is clear that the current bound is quite loose, e.g., $M_\eta \gtrsim 200$ GeV with $h_{\mu 1} = 1$ can be allowed.

Although the Yukawa interaction $\bar{L}_\mu \tilde{\eta}_1 N_i$ can not induce $\mu \to e\gamma$ at one-loop, it does contribute to muon anomalous magnetic moment [59]

$$\Delta a_\mu = -\sum_{i=1}^{2} \frac{|h_{\mu 1} V_{1i}|^2 M_\mu^2}{16\pi^2 M_{\eta_1}^2} F\left(\frac{M_{Ni}^2}{M_{\eta_1}^2}\right). \quad (19)$$

Comparing with $\mathrm{BR}(\tau \to \ell\gamma)$, there is no cancellations between the contributions of two N_i. However, the total contribution to Δa_μ is negative, while the observed discrepancy $\Delta a_\mu = a_\mu^{\mathrm{EXP}} - a_\mu^{\mathrm{SM}} = (261 \pm 78) \times 10^{-11}$ is positive [60]. Thus, the Yukawa interaction $\bar{L}_\mu \tilde{\eta}_1 N_{R1}$ can not explain the $(g-2)_\mu$ anomaly, and some other new physics is required [59]. On the other hand, since a too large negative contribution to Δa_μ is not favored, we consider a theoretical limit, i.e., $|\Delta a_\mu| < 10^{-10}$ in the following. The results are shown

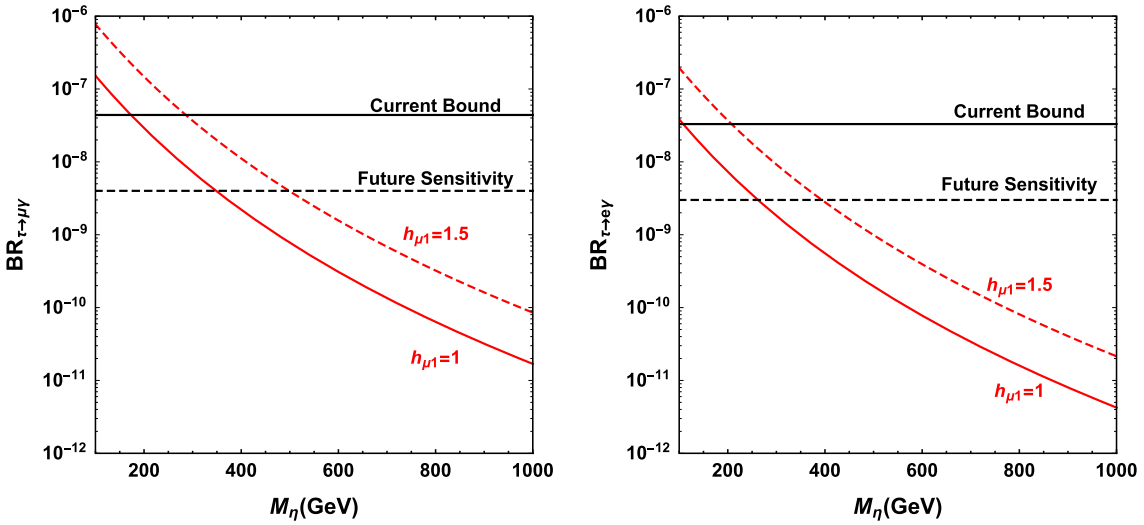

Fig. 3 Predictions for $\tau \to \mu\gamma$ (left) and $\tau \to e\gamma$ (right) with corresponding current bound [57] and future sensitivity [58]. In these figures, we have fixed $M_{N_1} = 200$ GeV

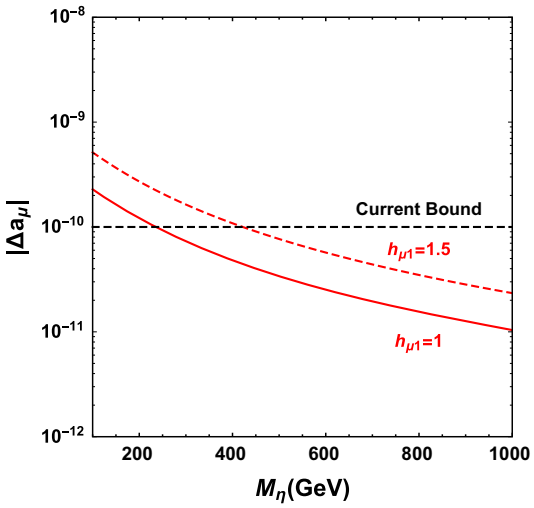

Fig. 4 Predictions for $|\Delta a_\mu|$. In this figures, we have fix $M_{N_1} = 200$ GeV

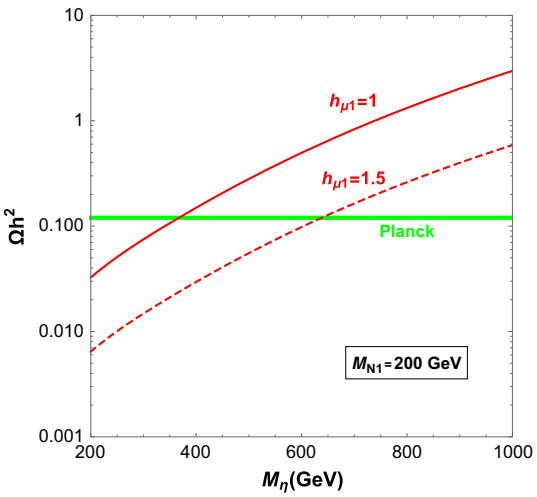

Fig. 5 Predicted relic density as a function of m_η, where we have fix $M_{N_1} = 200$ GeV. The green line corresponds to the observed relic density $\Omega h^2 = 0.120 \pm 0.001$ [48]

in Fig. 4. We find that the bound from $|\Delta a_\mu| < 10^{-10}$ is actually slightly more stringent than BR($\tau \to \mu\gamma$).

3.3 Dark matter

In this work, N_1 is the viable DM candidate. In the original scotogenic model [1], the possible annihilation channels are $N_1 N_1 \to \ell^+\ell^-, \bar{\nu}\nu$ via the Yukawa interaction $\bar{L}_\ell \tilde{\eta} N_1$ [61]. However, such annihilation channels are tightly constrained by non-observation of LFV [51]. Thanks to relative loose constraints from τ decays, the scanning results of Ref. [51] suggested that N_1 should have a large coupling to L_τ. Thus, the dominant annihilation channel is $\tau^+\tau^-$ and $\bar{\nu}_\tau \nu_\tau$ with $M_{N_1} \lesssim 3$ TeV.

Quite different from the original scotogenic model [1], the LFV process is either vanishing or suppressed in this flavor dependent model. As shown in Sect. 3.2, $\mathcal{O}(1)$ Yukawa couplings are allowed by current experimental bounds. In the following quantitative investigation, we consider a special scenario, i.e., $M_{\eta_1} = M_{\eta_2} = M_\eta$ for simplicity. In the limit of vanishing lepton masses, the Yukawa-portal annihilation cross section is [61,62]

$$\begin{aligned}\sigma v_{\rm rel} &= a + b v_{\rm rel}^2 \\ &= 0 + \sum_{\alpha,\beta} \left| h'_{\alpha 1} h'^*_{\beta 1} + f'_{\alpha 1} f'^*_{\beta 1} \right|^2 \frac{r^2(1-2r+2r^2)}{24\pi M_{N_1}^2} v_{\rm rel}^2,\end{aligned} \tag{20}$$

where $v_{\rm rel}$ is the relative speed, h' and f' are defined in Eq. (13), $r = M_{N_1}^2/(M_\eta^2 + M_{N_1}^2)$. The thermally averaged cross section is calculated as $\langle \sigma v_{\rm rel} \rangle = a + 6b/x_f$, where the freeze-out parameter $x_f = M_{N_1}/T_f$ is obtained by numerically solving

$$x_f = \ln\left(\frac{0.038 M_{\rm Pl} M_{N_1} \langle \sigma v_{\rm rel} \rangle}{\sqrt{g_* x_f}} \right). \tag{21}$$

The relic density is then calculated as [63]

$$\Omega h^2 = \frac{1.07 \times 10^9\ {\rm GeV}^{-1}}{M_{\rm Pl}} \frac{x_f}{\sqrt{g_*}} \frac{1}{a + 3b/x_f}, \tag{22}$$

where $M_{\rm Pl} = 1.22 \times 10^{19}$ GeV is the Planck mass, g_* is the number of relativistic degrees of freedom. The numerical results are depicted in Fig. 5. Provided the mass of the DM candidate is $M_{N_1} = 200$ GeV, then the observed relic density is interpreted by $h_{\mu 1} = 1$, $M_\eta = 366$ GeV or $h_{\mu 1} = 1.5$, $M_\eta = 640$ GeV. That is to say, $h_{\mu 1} \sim \mathcal{O}(1)$ is required to obtain correct relic density, and the larger $h_{\mu 1}$ is, the larger the mass splitting $M_\eta - M_{N_1}$ is.

In addition to the Yukawa-portal interaction, N_1 can also annihilate via the Higgs-portal and Z'-portal interactions [64–73]. In these two scenarios, $M_{N_1} \simeq M_{h,H}/2$ or $\simeq M_{Z'}/2$ are usually required to obtain correct relic density [74]. If the additional scalar singlet scalar H is lighter than N_1, then the annihilation channel $N_1 N_1 \to HH$ with $H \to b\bar{b}$ is able to explain the Fermi-LAT gamma-ray excess at the Galactic center [75,76].

The spin-independent DM-nucleon scattering cross section is dominantly mediated by scalar interactions, which is given by

$$\sigma^{\rm SI} = \frac{4}{\pi} \left(\frac{M_p M_{N_1}}{M_p + M_{N_1}} \right)^2 f_p^2, \tag{23}$$

where M_p is the proton mass and the hadronic matrix element f_p reads

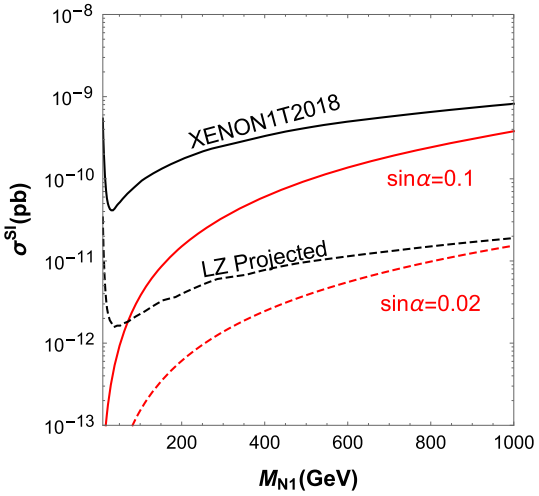

Fig. 6 Spin-independent cross section as a function of M_{N_1}. The black solid and dashed line correspond to current XENON1T [78] and future LZ [79] limits, respectively. In this figure, we have set $M_{H_1} = 500$ GeV and $v_S = 10$ TeV

$$\frac{f_p}{M_p} = \sum_{q=u,d,s} f_{Tq}^p \frac{\alpha_q}{M_q} + \frac{2}{27}\left(1 - \sum_{q=u,d,s} f_{Tq}^p\right) \sum_{q=c,b,t} \frac{\alpha_q}{M_q}. \tag{24}$$

and the effective vertex

$$\frac{\alpha_q}{M_q} = -\frac{y_{N_1}}{\sqrt{2}v} \sin 2\alpha \left(\frac{1}{M_h^2} - \frac{1}{M_{H_1}^2}\right), \tag{25}$$

Here, $y_{N_1} = y_{11} V_{11}^2$ is the effective Yukawa coupling of N_1 with S_1. For the proton, the parameters f_{Tq}^p are evaluated as $f_{Tu}^p = 0.020 \pm 0.004$, $f_{Td}^p = 0.026 \pm 0.005$ and $f_{Ts}^p = 0.118 \pm 0.062$ [77]. Figure 6 shows the numerical results for direct detection. It is obvious that the predicted $\sigma^{\rm SI}$ with $\sin\alpha = 0.1$ lies below current XENON1T limit, but the range of $M_{N_1} \gtrsim 70$ GeV is within future LZ's reach. However, if no direct detection signal is observed by LZ, then $\sin\alpha \lesssim 0.02$ should be satisfied.

In Fig. 7, we show the combined results from LFV, $|\Delta a_\mu|$, relic density and LHC search. In left pattern of Fig. 7, it indicates that for $M_{N_1} = 200$ GeV, the only exclusion region is from LHC search. Hence, either $M_\eta \lesssim 300$ GeV with $h_{\mu 1} \lesssim 0.9$ or $M_\eta \gtrsim 500$ GeV with $h_{\mu 1} \gtrsim 1.3$ is required. In right pattern of Fig. 7, two benchmark value $h_{\mu 1} = 1.0, 1.5$ are chosen to illustrate. For $h_{\mu 1} = 1.0$, we have 250 GeV $\lesssim M_{N_1} \lesssim M_\eta \sim 400$ GeV. Therefore, the only viable region is $M_{N_1} \sim M_\eta \lesssim 400$ GeV for $h_{\mu 1} \lesssim 1$. Meanwhile for $h_{\mu 1} = 1.5$, $M_{N_1} \gtrsim 120$ GeV with $M_\eta \gtrsim 520$ GeV is able to escape LHC limit.

3.4 Collider signature

In this part, we highlight some interesting collider signatures. Begin with the newly discovered 125 GeV Higgs boson h [80,81]. The existence of Majoron J will induce the invisible decay of SM Higgs via $h \to JJ$ [82]. The corresponding decay width is evaluated as

$$\Gamma(h \to JJ) \simeq \frac{M_h^3 \sin^2\alpha}{32\pi v_S^2}. \tag{26}$$

Then, the branching ratio of invisible decay is $\mathrm{BR}(h \to JJ) = \Gamma(h \to JJ)/(\Gamma(h \to JJ) + \Gamma_{\rm SM}\cos^2\alpha)$, where $\Gamma_{\rm SM} = 4.09$ MeV [83]. Currently, the combined direct

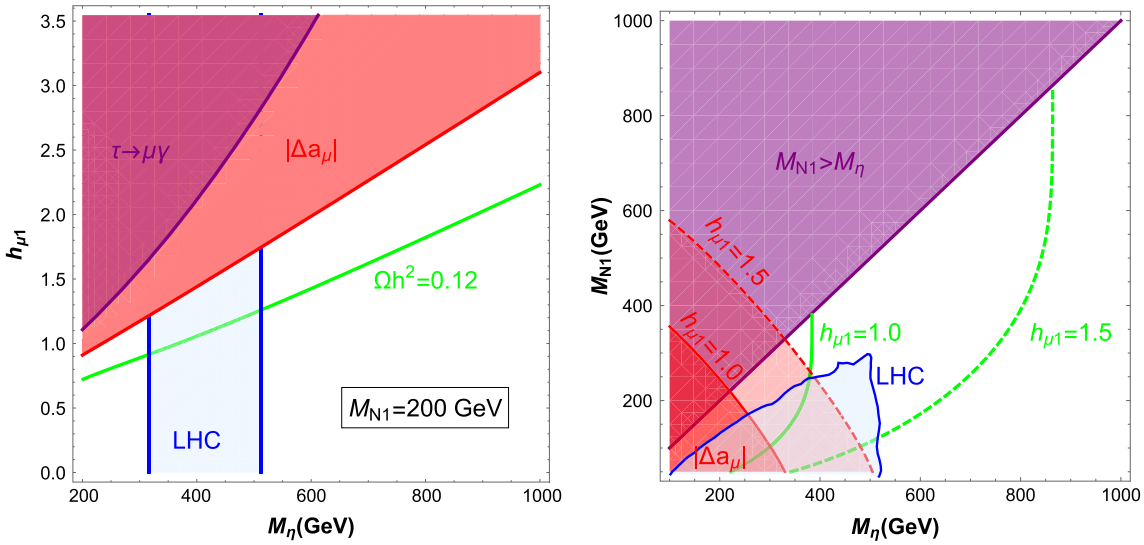

Fig. 7 Combined results for the Yukawa-portal DM. Left pattern: in the $h_{\mu 1}$-M_η plane; right pattern: in the M_{N_1}-M_η plane. The green lines satisfy the condition for correct relic density. And the blue regions are excluded by LHC direct search, which will be discussed in Sect. 3.4

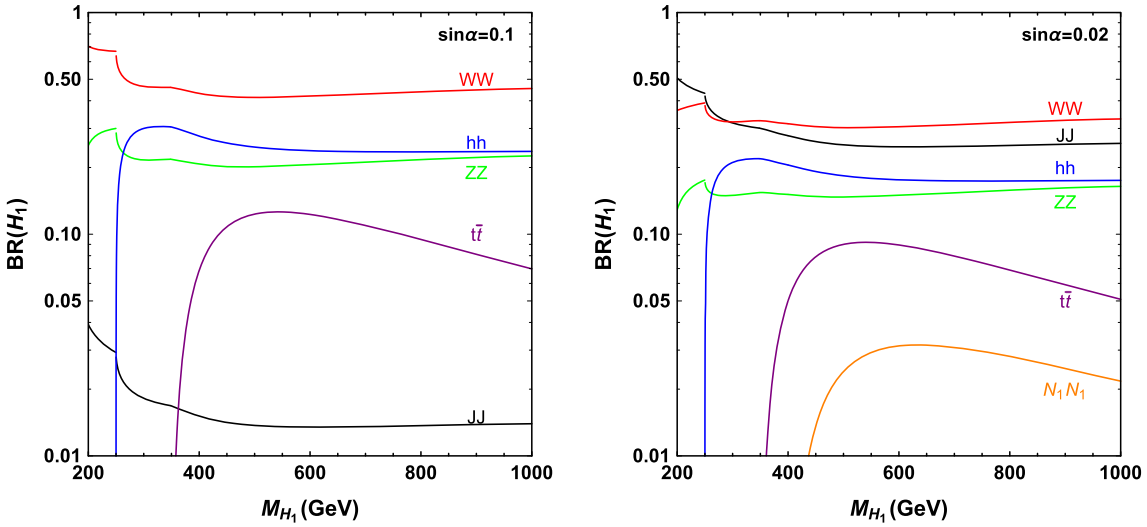

Fig. 8 Branching ratios of scalar singlet H_1 for $\sin\alpha = 0.1$ (left) and $\sin\alpha = 0.02$ (right). In this figures, we have also fix $M_{N_1} = 200$ GeV and $v_S = 10$ TeV. Note in left pattern, $\mathrm{BR}(H_1 \to N_1 N_1)$ is less than 0.01, thus is not shown in the plot

and indirect observational limit on invisible Higgs decay is $\mathrm{BR}(h \to JJ) < 0.24$ [84]. Typically for $\sin\alpha = 0.1$, $v_S = 10$ TeV, we have $\mathrm{BR}(h \to JJ) = 4.8 \times 10^{-4}$, which is far below current limit. Meanwhile, if $M_{H_1} < 2M_h$, then $h \to H_1 H_1$ with $H_1 \to JJ$ will also contribute to invisible Higgs decay [85].

In this paper, we consider the high mass scenario $M_{H_1} > M_h$. In addition to the usual $H_1 \to$ SM final states as real singlet model [86], the heavy scalar singlet can also decay into Majoron pair $H_1 \to JJ$ and DM pair $H_1 \to N_1 N_1$. Fig. 8 shows the dominant decay branching ratios of H_1. The invisible $\mathrm{BR}(H_1 \to JJ)$ is less than 0.02 when $\sin\alpha = 0.1$, therefore H_1 appears as a SM heavy Higgs with $\mathrm{BR}(H_1 \to hh) \approx \mathrm{BR}(h \to ZZ) \approx \frac{1}{2}\mathrm{BR}(H_1 \to WW) \approx \frac{1}{4}$. While for $\sin\alpha = 0.02$, the invisible $\mathrm{BR}(H_1 \to JJ)$ increases to about 0.25, reaching the same order of visible VV, hh decay. And the other invisible decay $H_1 \to N_1 N_1$ maximally reaches about 0.03 at $M_{H_1} \sim 600$ GeV. The dominant production channel of H_1 is via gluon fusion at LHC, which can be estimated as

$$\sigma(gg \to H_1) \approx \sin^2\alpha \times \sigma(gg \to h), \tag{27}$$

where $\sigma(gg \to h)$ is the SM Higgs production cross section but calculated with $M_h = M_{H_1}$. At present, $\sin\alpha \sim 0.1$ [87] leads to the promising signatures as $H_1 \to WW \to e\nu\mu\nu$ [88], $ZZ \to 4\ell$ [89] and $hh \to 2b2\gamma$ [90,91], etc. In the future, if no DM direct detection signal is observed, then the signature of heavy scalar H_1 will be much suppressed by tiny value of $\sin\alpha$.

Next, we discuss the gauge boson Z' associated with $U(1)_{B-2L_e-L_\tau}$. Its decay branching ratios are flavor-dependent, which makes it quite easy to distinguish from the flavor-universal ones, such as Z' from $U(1)_{B-L}$ [92]. Considering the heavy Z' limit, its partial decay width into fermion and scalar pairs are given by

$$\Gamma(Z' \to f\bar{f}) = \frac{M_{Z'}}{24\pi} g'^2 N_C^f (Q_{fL}^2 + Q_{fR}^2), \tag{28}$$

$$\Gamma(Z' \to SS^*) = \frac{M_{Z'}}{48\pi} g'^2 Q_S^2, \tag{29}$$

where N_C^f is the number of colours of the fermion f, i.e., $N_C^{l,\nu} = 1$, $N_C^q = 3$, and Q_X is the $U(1)_{B-2L_e-L_\tau}$ charge of particle X. In Table 4, we present the branching ratio of Z'. The dominant channel is $Z' \to e^+e^-$ with branching ratio of 0.308, and no $Z' \to \mu^+\mu^-$. The $B - 2L_e - L_\tau$ nature of Z' predicts definite relation between quark and lepton final states, e.g.,

$$\begin{aligned}&\mathrm{BR}(Z' \to b\bar{b}) : \mathrm{BR}(Z' \to e^+e^-)\\ &\quad : \mathrm{BR}(Z' \to \mu^+\mu^-) : \mathrm{BR}(Z' \to \tau^+\tau^-) = \frac{1}{3} : 4 : 0 : 1,\end{aligned} \tag{30}$$

which is also an intrinsic property to distinguish Z' of $U(1)_{B-2L_e-L_\tau}$ from other flavored gauge bosons [93].

In the framework of $U(1)_{B-2L_e-L_\tau}$, one important constraint on Z' comes from the precise measurement of four-fermion interactions at LEP [94], which requires

$$\frac{M_{Z'}}{g'} \gtrsim 7 \text{ TeV}. \tag{31}$$

Table 4 Decay branching ratio of $U(1)_{B-2L_e-L_\tau}$ gauge boson Z', where we have show the lepton flavor individually

$q\bar{q}$	e^+e^-	$\mu^+\mu^-$	$\tau^+\tau^-$	$\nu\nu$	NN	H_1H_1
0.154	0.308	0	0.077	0.192	0.192	0.077

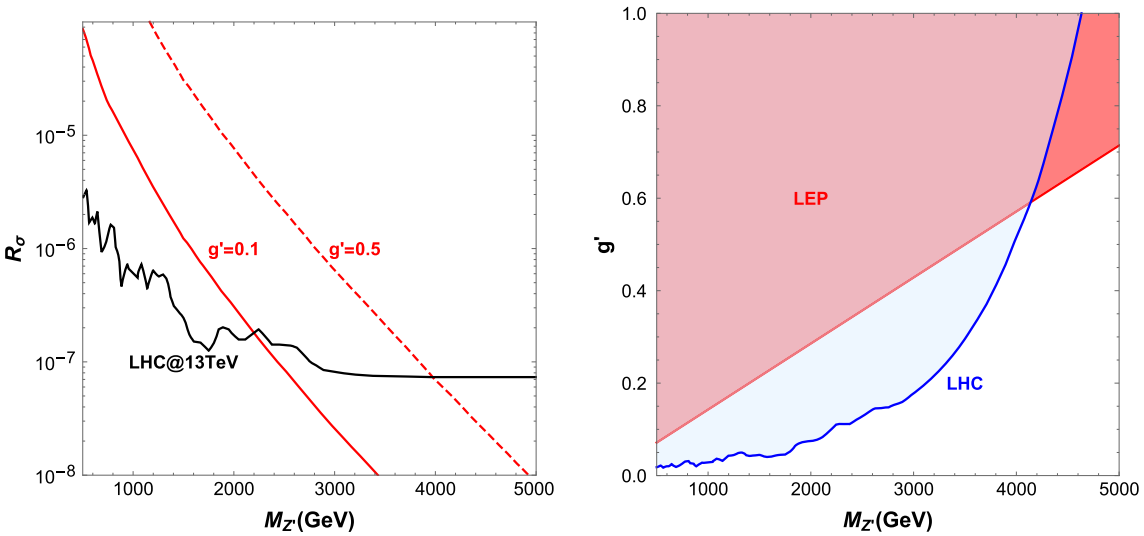

Fig. 9 Left pattern: predicted cross section ratios in $U(1)_{B-2L_e-L_\tau}$ and corresponding limit from LHC. Right pattern: allowed parameter space in the g'-$M_{Z'}$ plane

Since Z' couples to both quarks and leptons, the most promising signature at LHC is the dilepton signature $pp \to Z' \to e^+e^-$. Searches for such dilepton signature have been performed by ATLAS [95,96] and CMS collaboration [97]. Because of no $Z' \to \mu^+\mu^-$ channel, we can only take the results from CMS, which provides a limit on the ratio

$$R_\sigma = \frac{\sigma(pp \to Z' + X \to e^+e^- + X)}{\sigma(pp \to Z + X \to e^+e^- + X)}. \tag{32}$$

The theoretical cross section of the dilepton signature are calculated by using `MadGraph5_aMC@NLO` [98]. Left pattern of Fig. 9 shows that the dilepton signature has excluded $M_{Z'} \lesssim 2.2(4.0)$ TeV for $g' = 0.1(0.5)$. Then comparing the theoretical ratio with experimental limit, one can acquire the exclusion limit in the $g' - M_{Z'}$ plane as shown in right pattern of Fig. 9. Obviously, LHC limit is more stringent than LEP when $M_{Z'} \lesssim 4$ TeV.

The inert charge scalars $\eta^\pm_{1,2}$ are also observable at LHC. They can decay into charged leptons and right-hand singlets via the Yukawa interactions as

$$\Gamma(\eta_1^\pm \to \ell^\pm N_i) = \frac{M_{\eta_1^\pm}}{16\pi} |h'_{\ell i}|^2 \left(1 - \frac{M_{N_i}^2}{M_{\eta_1^\pm}^2}\right)^2, \tag{33}$$

$$\Gamma(\eta_2^\pm \to \ell^\pm N_i) = \frac{M_{\eta_1^\pm}}{16\pi} |f'_{\ell i}|^2 \left(1 - \frac{M_{N_i}^2}{M_{\eta_2^\pm}^2}\right)^2. \tag{34}$$

From Eq. (9), we aware that $\eta_1^\pm$ decays into μ, τ final states, while $\eta_2^\pm$ decays into e, τ final states. The electron-phobic nature of $\eta_1^\pm$ and muon-phobic nature of $\eta_2^\pm$ make them quite easy to distinguish. Meanwhile, their decay branching ratios are related by neutrino oscillation data through the Yukawa coupling h', f'. Considering the benchmark point in Eq. (15), the predicted branching ratios are shown in Table 5 in the heavy scalar limit. The dominant decay channel of $\eta_1^\pm$ is $\mu^\pm N_1$, and $\tau^\pm N_1$ for $\eta_2^\pm$. So $\eta_1^\pm$ is expected easier to be discovered. Produced via the Drell-Yan process $pp \to \eta_1^+\eta_1^-, \eta_2^+\eta_2^-$, the decay channel $\eta^\pm_{1,2} \to \ell^\pm N_1$ then leads to signature $\ell^+\ell^- + \not{E}_T$. Exclusion region by direct LHC search for such signature [99] has been shown in right pattern of Fig. 7. To satisfy the direct LHC search bounds, one needs either $M_{N_1} \lesssim M_\eta < 500$ GeV or $M_\eta > 500$ GeV.

Table 5 Branching ratios of charge scalar $\eta^\pm_{1,2}$

Final state	$e^\pm N_1$	$\mu^\pm N_1$	$\tau^\pm N_1$	$e^\pm N_2$	$\mu^\pm N_2$	$\tau^\pm N_2$
$\eta_1^\pm$	0.000	0.465	0.099	0.000	0.178	0.258
$\eta_2^\pm$	0.043	0.000	0.611	0.113	0.000	0.233

4 Conclusion

The scotogenic model is an elegant pathway to explain the origin of neutrino mass and dark matter. Meanwhile, texture-zeros in neutrino mass matrix provide a promising way to under stand the leptonic flavor structure. Therefore, it is appealing to connect the scotogenic model with texture-zeros. In this paper, we propose a viable approach to realise two texture-zeros in the scotogenic model with flavor dependent $U(1)_{B-2L_\alpha-L_\beta}$ gauge symmetry. These models are extended by two right-handed singlets N_{Ri} and two inert scalar doublets η_i, which are odd under the dark Z_2 symmetry. Six kinds of texture-zeros are realised in our approach, i.e., texture A_1, A_2, B_3, B_4, D_1 and D_2. Among all the six

texture-zeros, we find that texture A_1 and A_2 are allowed by current experimental limits, while texture B_3 and B_4 are marginally allowed. Besides, texture D_1 and D_2 are already excluded by neutrino oscillation data.

Realization of texture-zeros in the scotogenic model makes the model quite predictive. And we have taken texture A_1 derived from $U(1)_{B-2L_e-L_\tau}$ for illustration. Some distinct features are summarized in the following:

- The texture A_1 predicts vanishing neutrinoless double beta decay rate. And only normal neutrino mass hierarchy is allowed. It predicts $m_1 \sim 0.007$ eV, $m_2 \sim 0.01$ eV, and $m_3 \approx \sqrt{\Delta m^2} \sim 0.05$ eV, then $\sum m_i \sim 0.07$ eV. There are also strong correlation between the Dirac and Majorana phases, i.e., $\rho \approx \frac{\delta}{2}$ and $\sigma \approx \frac{\delta}{2} - \frac{\pi}{2}$.
- The ratios of corresponding Yukawa couplings are also predicted by neutrino oscillation data, e.g.,

$$\frac{h_{\tau 2}}{h_{\mu 1}} : \frac{f_{\tau 1}}{h_{\mu 1}} : \frac{f_{e2}}{h_{\mu 1}} \simeq 0.745 : 0.933 : 0.401.$$

- Due to specific Yukawa structure, the LFV process $\mu \to e\gamma$ is missing at one-loop level. Meanwhile, large cancellations are possible for $\tau \to \mu\gamma$ and $\tau \to e\gamma$ with degenerate right-handed singlets. More stringent constraint comes from muon anomalous magnetic moment Δa_μ. Although $\mathcal{O}(1)$ Yukawa couplings are easily to avoid such limit.
- Satisfying all constraints, correct relic density of dark matter N_1 is achieved for $M_{N_1} \lesssim M_\eta < 500$ GeV with $h_{\mu 1} \lesssim 1$ or $M_\eta > 500$ GeV with $h_{\mu 1} > 1$.As for direct detection, we have shown that the predicted spin-independent DM-nucleon cross section $\sigma^{\rm SI}$ with $\sin\alpha = 0.1$ satisfies the current XENON1T limit, but is within future reach of LZ.
- The Majoron J contributes to invisible decay of SM Higgs. The additional scalar singlet H_1 can be probe in the channel $gg \to H_1 \to W^+W^-, ZZ$ at LHC. Decays of charged scalars $\eta^\pm_{1,2}$ lead to $pp \to \eta^+_{1,2}\eta^-_{1,2} \to \ell^+\ell^- + \not{E}_T$ signature. Note that the corresponding branching ratios are also correlated with neutrino oscillation parameters.
- The neutral gauge boson Z' is promising via the di-electron signature $pp \to Z' \to e^+e^-$. Its $B - 2L_e - L_\tau$ nature can be confirmed by

$$\begin{aligned}&\mathrm{BR}(Z' \to b\bar{b}) : \mathrm{BR}(Z' \to e^+e^-) : \mathrm{BR}(Z' \to \mu^+\mu^-)\\ &: \mathrm{BR}(Z' \to \tau^+\tau^-) = \frac{1}{3} : 4 : 0 : 1,\end{aligned}$$

In a nutshell, the scotogenic model with flavor dependent $U(1)_{B-2L_\alpha-L_\beta}$ symmetry predicts distinct and observable phenomenology, which is useful to distinguish from other models.

Acknowledgements The work of Weijian Wang is supported by National Natural Science Foundation of China under Grant Numbers 11505062, Special Fund of Theoretical Physics under Grant Numbers 11447117 and Fundamental Research Funds for the Central Universities under Grant Numbers 2014ZD42. The work of Zhi-Long Han is supported by National Natural Science Foundation of China under Grant Nos. 11805081 and 11605075, Natural Science Foundation of Shandong Province under Grant Nos. ZR2019QA021, ZR2018MA047, ZR2017JL006 and ZR2014AM016.

Data Availability Statement This manuscript has no associated data or the data will not be deposited. [Authors' comment: The data can be directly read from the figures.]

References

1. E. Ma, Phys. Rev. D **73**, 077301 (2006). arXiv:hep-ph/0601225
2. L.M. Krauss, S. Nasri, M. Trodden, Phys. Rev. D **67**, 085002 (2003). arXiv:hep-ph/0210389
3. M. Aoki, S. Kanemura, O. Seto, Phys. Rev. Lett. **102**, 051805 (2009). arXiv:0807.0361 [hep-ph]
4. E. Ma, Mod. Phys. Lett. A **21**, 1777 (2006). arXiv:hep-ph/0605180
5. T. Hambye, K. Kannike, E. Ma, M. Raidal, Phys. Rev. D **75**, 095003 (2007). arXiv:hep-ph/0609228
6. D. Aristizabal Sierra, J. Kubo, D. Restrepo, D. Suematsu, O. Zapata, Phys. Rev. D **79**, 013011 (2009). arXiv:0808.3340 [hep-ph]
7. D. Suematsu, T. Toma, T. Yoshida, Phys. Rev. D **79**, 093004 (2009). arXiv:0903.0287 [hep-ph]
8. D. Schmidt, T. Schwetz, T. Toma, Phys. Rev. D **85**, 073009 (2012). arXiv:1201.0906 [hep-ph]
9. R. Bouchand, A. Merle, JHEP **1207**, 084 (2012). arXiv:1205.0008 [hep-ph]
10. A. Merle, M. Platscher, JHEP **1511**, 148 (2015). arXiv:1507.06314 [hep-ph]
11. E. Ma, A. Natale, A. Rashed, Int. J. Mod. Phys. A **27**, 1250134 (2012). arXiv:1206.1570 [hep-ph]
12. M. Klasen, C.E. Yaguna, J.D. Ruiz-Alvarez, D. Restrepo, O. Zapata, JCAP **1304**, 044 (2013). arXiv:1302.5298 [hep-ph]
13. S.Y. Ho, J. Tandean, Phys. Rev. D **87**, 095015 (2013). arXiv:1303.5700 [hep-ph]
14. A. Ahriche, S. Nasri, JCAP **1307**, 035 (2013). arXiv:1304.2055 [hep-ph]
15. M. Chekkal, A. Ahriche, A.B. Hammou, S. Nasri, Phys. Rev. D **95**(9), 095025 (2017). arXiv:1702.04399 [hep-ph]
16. K.P. Modak, JHEP **1503**, 064 (2015). arXiv:1404.3676 [hep-ph]
17. E. Molinaro, C.E. Yaguna, O. Zapata, JCAP **1407**, 015 (2014). arXiv:1405.1259 [hep-ph]
18. G. Faisel, S.Y. Ho, J. Tandean, Phys. Lett. B **738**, 380 (2014). arXiv:1408.5887 [hep-ph]
19. A. Merle, M. Platscher, Phys. Rev. D **92**(9), 095002 (2015). arXiv:1502.03098 [hep-ph]

20. A. Ahriche, K.L. McDonald, S. Nasri, JHEP **1602**, 038 (2016). arXiv:1508.02607 [hep-ph]
21. A. Ahriche, K.L. McDonald, S. Nasri, JHEP **1606**, 182 (2016). arXiv:1604.05569 [hep-ph]
22. A. Ahriche, A. Manning, K.L. McDonald, S. Nasri, Phys. Rev. D **94**(5), 053005 (2016). arXiv:1604.05995 [hep-ph]
23. M. Lindner, M. Platscher, C.E. Yaguna, A. Merle, Phys. Rev. D **94**(11), 115027 (2016). arXiv:1608.00577 [hep-ph]
24. A.G. Hessler, A. Ibarra, E. Molinaro, S. Vogl, JHEP **1701**, 100 (2017). arXiv:1611.09540 [hep-ph]
25. D. Borah, A. Gupta, Phys. Rev. D **96**(11), 115012 (2017). arXiv:1706.05034 [hep-ph]
26. A. Abada, T. Toma, JHEP **1804**, 030 (2018). arXiv:1802.00007 [hep-ph]
27. T. Hugle, M. Platscher, K. Schmitz, Phys. Rev. D **98**(2), 023020 (2018). arXiv:1804.09660 [hep-ph]
28. S. Baumholzer, V. Brdar, P. Schwaller, JHEP **1808**, 067 (2018). arXiv:1806.06864 [hep-ph]
29. D. Borah, P.S.B. Dev, A. Kumar, arXiv:1810.03645 [hep-ph]
30. L. Bian, X. Liu, arXiv:1811.03279 [hep-ph]
31. E. Ma, I. Picek, B. Radovčič, Phys. Lett. B **726**, 744 (2013). arXiv:1308.5313 [hep-ph]
32. Y. Cai, J. Herrero-García, M.A. Schmidt, A. Vicente, R.R. Volkas, Front. Phys. **5**, 63 (2017). arXiv:1706.08524 [hep-ph]
33. P.H. Frampton, S.L. Glashow, D. Marfatia, Phys. Lett. B **536**, 79 (2002). arXiv:hep-ph/0201008]
34. H. Fritzsch, Z.Z. Xing, JHEP **1109**, 083 (2011). arXiv:1108.4534 [hep-ph]
35. J. Alcaide, J. Salvado, A. Santamaria, JHEP **1807**, 164 (2018). arXiv:1806.06785 [hep-ph]
36. W. Grimus, A.S. Joshipura, L. Lavoura, M. Tanimoto, Eur. Phys. J. C **36**, 227 (2004). arXiv:hep-ph/0405016
37. T. Araki, J. Heeck, J. Kubo, JHEP **1207**, 083 (2012). arXiv:1203.4951 [hep-ph]
38. L.M. Cebola, D. Emmanuel-Costa, R. Gonzalez Felipe, Phys. Rev. D **88**(11), 116008 (2013). arXiv:1309.1709 [hep-ph]
39. T. Kitabayashi, Phys. Rev. D **98**(8), 083011 (2018). arXiv:1808.01060 [hep-ph]
40. T. Kitabayashi, S. Ohkawa, M. Yasuè, Int. J. Mod. Phys. A **32**(32), 1750186 (2017). arXiv:1703.09417 [hep-ph]
41. S. Baek, H. Okada, K. Yagyu, JHEP **1504**, 049 (2015). arXiv:1501.01530 [hep-ph]
42. S. Baek, Phys. Lett. B **756**, 1 (2016). arXiv:1510.02168 [hep-ph]
43. S. Lee, T. Nomura, H. Okada, Nucl. Phys. B **931**, 179 (2018). arXiv:1702.03733 [hep-ph]
44. K. Asai, K. Hamaguchi, N. Nagata, S.Y. Tseng, K. Tsumura, arXiv:1811.07571 [hep-ph]
45. T. Nomura, H. Okada, Phys. Dark Univ. **21**, 90 (2018). arXiv:1712.00941 [hep-ph]
46. P. Ko, T. Nomura, H. Okada, Phys. Lett. B **772**, 547 (2017). arXiv:1701.05788 [hep-ph]
47. T. Nomura, H. Okada, arXiv:1806.09957 [hep-ph]
48. N. Aghanim et al. [Planck Collaboration], arXiv:1807.06209 [astro-ph.CO]
49. I. Esteban, M.C. Gonzalez-Garcia, A. Hernandez-Cabezudo, M. Maltoni, T. Schwetz, arXiv:1811.05487 [hep-ph]
50. E.I. Lashin, N. Chamoun, Phys. Rev. D **85**, 113011 (2012). arXiv:1108.4010 [hep-ph]
51. A. Vicente, C.E. Yaguna, JHEP **1502**, 144 (2015). arXiv:1412.2545 [hep-ph]
52. S.M. Bilenky, C. Giunti, W. Grimus, B. Kayser, S.T. Petcov, Phys. Lett. B **465**, 193 (1999). arXiv:hep-ph/9907234]
53. F. Vissani, JHEP **9906**, 022 (1999). arXiv:hep-ph/9906525]
54. S. Vagnozzi, E. Giusarma, O. Mena, K. Freese, M. Gerbino, S. Ho, M. Lattanzi, Phys. Rev. D **96**(12), 123503 (2017). arXiv:1701.08172 [astro-ph.CO]
55. T. Toma, A. Vicente, JHEP **1401**, 160 (2014). arXiv:1312.2840 [hep-ph]
56. R. Ding, Z.L. Han, Y. Liao, H.J. Liu, J.Y. Liu, Phys. Rev. D **89**(11), 115024 (2014). arXiv:1403.2040 [hep-ph]
57. B. Aubert et al., BaBar Collaboration, Phys. Rev. Lett. **104**, 021802 (2010). arXiv:0908.2381 [hep-ex]
58. K. Hayasaka [Belle and Belle-II Collaborations], J. Phys. Conf. Ser. **408**, 012069 (2013)
59. M. Lindner, M. Platscher, F.S. Queiroz, Phys. Rept. **731**, 1 (2018). arXiv:1610.06587 [hep-ph]
60. T. Blum, A. Denig, I. Logashenko, E. de Rafael, B.L. Roberts, T. Teubner, G. Venanzoni, arXiv:1311.2198 [hep-ph]
61. J. Kubo, E. Ma, D. Suematsu, Phys. Lett. B **642**, 18 (2006). arXiv:hep-ph/0604114
62. T. Li, W. Chao, Nucl. Phys. B **843**, 396 (2011). arXiv:1004.0296 [hep-ph]
63. G. Bertone, D. Hooper, J. Silk, Phys. Rept. **405**, 279 (2005). arXiv:hep-ph/0404175]
64. N. Okada, O. Seto, Phys. Rev. D **82**, 023507 (2010). arXiv:1002.2525 [hep-ph]
65. S. Kanemura, O. Seto, T. Shimomura, Phys. Rev. D **84**, 016004 (2011). arXiv:1101.5713 [hep-ph]
66. N. Okada, Y. Orikasa, Phys. Rev. D **85**, 115006 (2012). arXiv:1202.1405 [hep-ph]
67. W. Wang, Z.L. Han, Phys. Rev. D **92**, 095001 (2015). arXiv:1508.00706 [hep-ph]
68. N. Okada, S. Okada, Phys. Rev. D **93**(7), 075003 (2016). arXiv:1601.07526 [hep-ph]
69. N. Okada, S. Okada, D. Raut, Phys. Lett. B **780**, 422 (2018). arXiv:1712.05290 [hep-ph]
70. Z.L. Han, W. Wang, R. Ding, Eur. Phys. J. C **78**(3), 216 (2018). arXiv:1712.05722 [hep-ph]
71. S. Okada, Adv. High Energy Phys. **2018**, 5340935 (2018). arXiv:1803.06793 [hep-ph]
72. Z.L. Han, W. Wang, Eur. Phys. J. C **78**(10), 839 (2018). arXiv:1805.02025 [hep-ph]
73. N. Okada, S. Okada, D. Raut, arXiv:1811.11927 [hep-ph]
74. D. Borah, D. Nanda, N. Narendra, N. Sahu, arXiv:1810.12920 [hep-ph]
75. Y.G. Kim, K.Y. Lee, C.B. Park, S. Shin, Phys. Rev. D **93**(7), 075023 (2016). arXiv:1601.05089 [hep-ph]
76. R. Ding, Z.L. Han, L. Huang, Y. Liao, Chin. Phys. C **42**(10), 103101 (2018). arXiv:1802.05248 [hep-ph]
77. J.R. Ellis, A. Ferstl, K.A. Olive, Phys. Lett. B **481**, 304 (2000). arXiv:hep-ph/0001005
78. E. Aprile et al. [XENON Collaboration], Phys. Rev. Lett. **121**(11), 111302 (2018). arXiv:1805.12562 [astro-ph.CO]
79. D.S. Akerib et al. [LUX-ZEPLIN Collaboration], arXiv:1802.06039 [astro-ph.IM]
80. G. Aad et al., ATLAS Collaboration, Phys. Lett. B **716**, 1 (2012). arXiv:1207.7214 [hep-ex]
81. S. Chatrchyan et al., CMS Collaboration, Phys. Lett. B **716**, 30 (2012). arXiv:1207.7235 [hep-ex]
82. W. Wang, Z.L. Han, Phys. Rev. D **94**(5), 053015 (2016). arXiv:1605.00239 [hep-ph]
83. D. de Florian et al. [LHC Higgs Cross Section Working Group], arXiv:1610.07922 [hep-ph]
84. V. Khachatryan et al., CMS Collaboration, JHEP **1702**, 135 (2017). arXiv:1610.09218 [hep-ex]
85. C. Bonilla, J.W.F. Valle, J.C. Romão, Phys. Rev. D **91**(11), 113015 (2015). arXiv:1502.01649 [hep-ph]
86. T. Robens, T. Stefaniak, Eur. Phys. J. C **76**(5), 268 (2016). arXiv:1601.07880 [hep-ph]
87. A. Ilnicka, T. Robens, T. Stefaniak, Mod. Phys. Lett. A **33**(10–11), 1830007 (2018). arXiv:1803.03594 [hep-ph]

88. M. Aaboud et al. [ATLAS Collaboration], Eur. Phys. J. C **78**(1), 24 (2018). arXiv:1710.01123 [hep-ex]
89. M. Aaboud et al. [ATLAS Collaboration], Phys. Rev. D **98**(5), 052008 (2018). arXiv:1808.02380 [hep-ex]
90. A.M. Sirunyan et al., CMS Collaboration, Phys. Lett. B **788**, 7 (2019). arXiv:1806.00408 [hep-ex]
91. M. Aaboud et al., ATLAS Collaboration, JHEP **1811**, 040 (2018). arXiv:1807.04873 [hep-ex]
92. L. Basso, A. Belyaev, S. Moretti, C.H. Shepherd-Themistocleous, Phys. Rev. D **80**, 055030 (2009). arXiv:0812.4313 [hep-ph]
93. E.J. Chun, A. Das, J. Kim, J. Kim, arXiv:1811.04320 [hep-ph]
94. G. Cacciapaglia, C. Csaki, G. Marandella, A. Strumia, Phys. Rev. D **74**, 033011 (2006). arXiv:hep-ph/0604111
95. M. Aaboud et al., ATLAS Collaboration, JHEP **1710**, 182 (2017). arXiv:1707.02424 [hep-ex]
96. G. Aad et al. [ATLAS Collaboration], arXiv:1903.06248 [hep-ex]
97. A.M. Sirunyan et al., CMS Collaboration, JHEP **1806**, 120 (2018). arXiv:1803.06292 [hep-ex]
98. J. Alwall et al., JHEP **1407**, 079 (2014). arXiv:1405.0301 [hep-ph]
99. M. Aaboud et al. [ATLAS Collaboration], Eur. Phys. J. C **78**(12), 995 (2018). arXiv:1803.02762 [hep-ex]